A Prototype of a Linear Switched Reluctance Motor with a New Design Methodology

D.S.B. FONSECA C.P. CABRITA M.R.A. CALADO
Department of Electromechanical Engineering, CASE-Research Unit on Electrical Drives and Systems
University of Beira Interior
Calçada Fonte do Lameiro, P-6201-001 Covilhã
PORTUGAL
davide@ubi.pt http://dem.ubi.pt/~davide

Abstract - A new and original optimized design methodology concerning a Linear Switched Reluctance Machine (LSRM), with a new topology and for light electric traction applications, is proposed in this paper. This methodology is based on the systematic use of a simple geometric design process, and a fast simulation methodology is used to evaluate the performance of each one of the several design machines.

Key-Words - Linear Switched Reluctance Machines, Traction Forces Evaluation, Machine Simulation, Optimized Design.

LIST OF SYMBOLS

B	Magnetic flux density
H	Magnetic field intensity
b_p	Primary tooth length
b_s	Secondary tooth length
D_{cu}	Winding wire diameter
F	Average value of the developed force
g	Airgap length
h_b	Coil length
h_p	Primary slot depth
h_s	Secondary tooth depth
$i(x,\psi)$	Phase instantaneous current
I_{max}	Maximum rms value of the coil current
I_{pu}	Per unit rms current considering I_{max} value as base value
k_e	Slot fill factor
l_b	Coil width
m	Primary phase number
N	Number of turns per primary phase
N_2	Secondary pole number
N_{db}	Number of coils per primary teeth
N_{br}	Number of coils per winding parallel path
N_e	Number of turns per primary coil
N_r	Number of parallel paths of each primary phase
U_0	DC input voltage of power electronic converter
u	Input phase voltage
v	Machine linear speed, or velocity
w	Primary and secondary stack iron width
$W_m(x,\psi)$	Stored magnetic energy
x	Phase relative position considering the origin on one unaligned position
τ_P	Primary pole pitch
τ_S	Secondary pole pitch
ψ	Flux linkage
η	Expected efficiency
t	Time
μ_0	Free space magnetic permeability

1 Introduction

Usually linear machines are employed for straight line displacement applications. Because one wants a traction machine, then the topology shown in Fig. 1 become as a better option, because it presenting a cheap secondary and modular primary construction with articulated mechanical connection between primary phases (movable part) which increases significantly both the fault tolerance and the ability to bend.

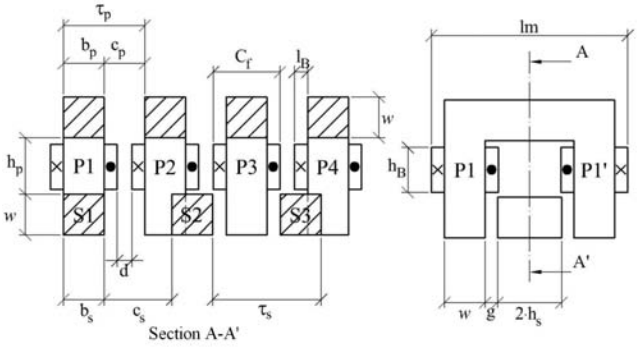

Fig.1 4-phase 8/6 Linear Switched Reluctance Machine geometry and envelope dimensions.

The LSRM optimized design consists to obtain the best performances concerning efficiency and specific power (mechanical output power to the weight ratio). On the other hand, the advantage of a computer simulation for the machine behavior in design process is well defined by T.J.E. Miller [1] "*Any switched reluctance motor operates in a series of strokes or transients and does not have a steady-state in which all variables are constant.... This means that for all except the most basic sizing calculations, computer-based design methods must incorporate simulation capability as an integral part of the design process.*"

The used simulation methodology is based on the knowledge of the magnetization characteristic B=f(H) of the used iron material, as well as on the calculated machine dimensions. The simulation methodology permits to obtain the machine magnetization curves based on these values as well as the linearization of the airgap length mean value between the unaligned and aligned positions [2].

2 Geometric design

By application of the Lawrenson's "feasible triangles" presented in Fig. 2, one obtains the following relationships:

$$b_S = C_P = b_P \quad (1)$$

$$\tau_P = b_P + C_p \quad (2)$$

$$\tau_S = b_S + C_S \quad (3)$$

$$C_m = 2m\tau_P = N_2\,\tau_S \quad (4)$$

$$C_S = \frac{b_P(4m - N_2)}{N_2} \quad (5)$$

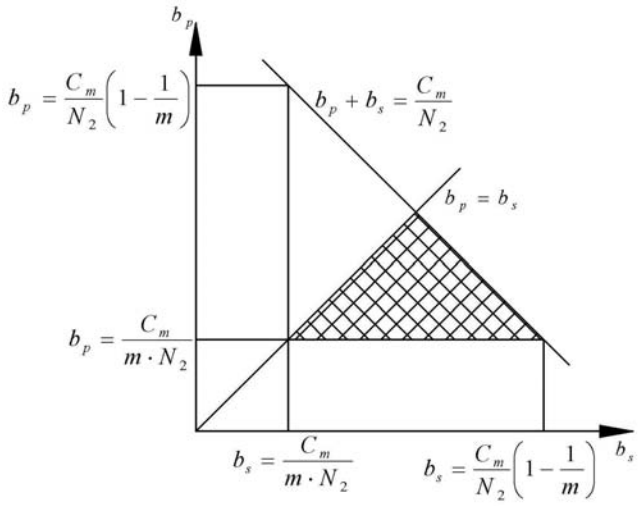

Fig.2 Lawrenson's "feasible triangle" for LSRM.

For rotating SRM is usual to consider the secondary tooth depth h_S between 20 to 30 times greater than the airgap length g. However, due to mechanical constraints, the linear machine airgap length must be significantly higher. Thus, h_S is equal to 10 to 15 times greater than g [2], as expressed in (6).

$$h_s = (10\ldots15)g \quad (6)$$

In this design methodology several combination of the remaining dimensions are explored and one of them is selected to be adopted. Thus, the minimum value of b_P is limited by maximum operation frequency of the power electronic converter and machine rated speed, and the minimum value of both primary and secondary stack iron width w is related to the mechanical stress resistance, namely because of the attraction forces between primary and secondary. In this prototype one have consider 18mm as the minimum value of both b_P and w.

As shown in [2] the control strategy adopted to be used at continuous rated regime is a single pulse operation with the turn on position equal to zero and commutation position equal to 40% of the secondary pole pitch.

To analyze w, b_P, g and N_e (number of turns per coil) and their influence on the machine performance, the winding wire diameter D_{cu} was chosen with the standard value of 0.5mm. Thus, the maximum rms value for the coil current is given by:

$$I_{max} = \frac{{D_{cu}}^2 \cdot 3.5 \cdot 10^6 \cdot \pi}{4} \quad (7)$$

Taking into account the supply voltage and the values of X_0 and X_C one can expect one average value of the phase input voltage about 30% of the supply voltage, i.e. 60V.

On the other hand, I_{max} is approximately 0.7A which gives 42W per parallel path.

Thus, once the desired machine is a 600W machine, corresponding to 150W per phase, then the phase winding must be composed by 4 parallel connected coils.

In order to provide space to accommodate the winding it is necessary to determine his cross section area, which is obtained according to the following relationship:

$$A_B = N_e \cdot N_{bd} \frac{\pi d_{cu}^2}{4 k_e} = l_B\, h_B \quad (8)$$

where the slot fill factor k_e is usually of the order of 0.4 for concentrated windings.

In addition, to avoid a large leakage flux, the following relationships should be respected:

$$l_B \le 1.3w \quad (9)$$

and

$$l_B \leq 1.3 b_p \tag{10}$$

3 Simulation methodology

For machine simulation one considers that all phase coils are series-connected, and the DC input voltage for power electronic energy converter is given by the following equation:

$$U = N_r \, U_0 \tag{11}$$

Independently of the chosen inverter topology, by application of the 2nd Kirchhoff's law one obtains the following time dependent equation for an excited phase circuit:

$$u(t) = R\, i(t) + \frac{\partial \psi(t)}{\partial t} \tag{12}$$

where R is the equivalent phase resistance given by:

$$R = N_r \cdot N_{br} \cdot R_{coil} \tag{13}$$

obtained from the coil resistance R_{coil}, according to:

$$R_{coil} = \frac{4 \rho N_e}{\pi \, D_{cu}{}^2} \left[2.2w + 0.9\pi (b_P + l_B) \right] \tag{14}$$

If one considers a constant linear speed v, then (12) can be rewritten as follows:

$$\frac{\partial \psi}{\partial x} = \frac{V(x) - R \cdot I(x,\psi)}{v} \tag{15}$$

Thus, knowing position, current and flux linkage values for a given position x_n, and applying the Runge-Kutta method to (15), and considering a step of Δx, one obtains:

$$\psi(x_{n+1}) = \psi(x_n) + \Delta\psi(x_n) \tag{16}$$

$$\Delta\psi(x_n) = \frac{\left[K_1(x_n) + 2K_2(x_n) + 2K_3(x_n) + K_4(x_n) \right]}{6} \tag{17}$$

$$K_1(x_n) = \frac{u(x_n) - R \cdot i\left[x_n, \psi(x_n) \right]}{v} \cdot \Delta x \tag{18}$$

$$K_2(x_n) = \frac{\Delta x}{v} \left[u(x_n) - R \cdot i\left[\left(x_n + \frac{\Delta x}{2} \right), \left(\psi(x_n) + \frac{K_1(x_n)}{2} \right) \right] \right] \tag{19}$$

$$K_3(x_n) = \frac{\Delta x}{v} \left[u(x_n) - R \cdot i\left[\left(x_n + \frac{\Delta x}{2} \right), \left(\psi(x_n) + \frac{K_2(x_n)}{2} \right) \right] \right] \tag{20}$$

$$K_4(x_n) = \frac{\Delta x}{v} \left[u(x_n) - R \cdot i\left[(x_n + \Delta x), (\psi(x_n) + K_3(x_n)) \right] \right] \tag{21}$$

Taking into account that the exposed method uses both the flux linkage and relative position as state variables, the developed force is derived from D'Lambert's principle as follows [3]:

$$f(x,\psi) = - \left. \frac{\partial W_m(x,\psi)}{\partial x} \right|_{\psi = \psi_J} \tag{22}$$

$$f(x,\psi) = \frac{W_m\left[(x - \Delta x), \psi \right] - W_m\left[(x + \Delta x), \psi \right]}{2 \cdot \Delta x} \tag{23}$$

where Δx should tend to zero and must be lower than x_n, and the phase stored magnetic energy W_m is obtained by the following relationship:

$$W_m(x, \psi_J) = \left. \int_{\psi=0}^{\psi=\psi_J} i(x,\psi) \partial\psi \right|_{x=Const.} \tag{24}$$

As can be seen, several values for current $i(x,\psi)$ and force $W_m(x,\psi)$ are necessary, being calculated by using the magnetization curves lookup table. Note that these necessary values obtained directly from a lookup table, are obtained from numerical interpolation using Cubic Spline Interpolation.

4 Magnetization curves

As explained, this simulation method requires the use of a lookup table representative of the magnetization curves.

For exact determination of the machine magnetization curves based on its dimensions there are two possible ways:

- from finite element analysis,
- from static test measurements [4].

In this work the used methodology to obtain the magnetization curves is presented in [5], and is made through the linearization of the airgap length mean value between the unaligned and aligned positions.

According to [5] and taking into account all series-connected phase coils, the following equations represent a simplest and fast method to obtain ψ from B=f(H) characteristic represented in Fig. 3:

$$\psi = N \, B \, w \, b_p, \tag{25}$$

where N is the number of turns per phase, given by:

$$N = N_r \, N_{br} \, N_e \tag{26}$$

Then, the input coil current for each relative position is obtained by using the following equation:

$$I(x,\psi)=\frac{H\,l_f(x)+\dfrac{\psi\,l_g(x)}{N\,wb_p\,\mu_0}}{N} \qquad (27)$$

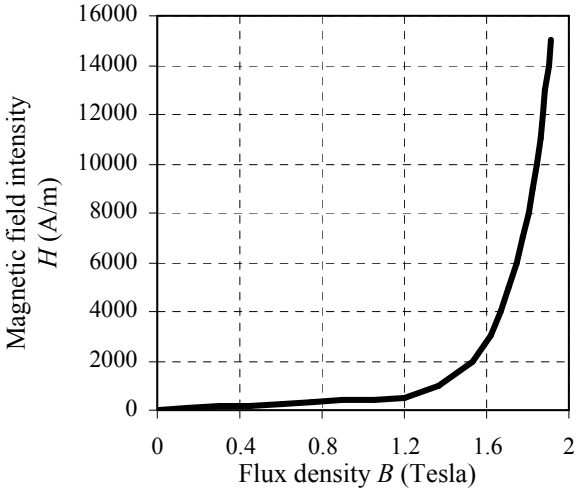

Fig.3 Magnetization curves for the magnetic circuit material.

where l_g and l_f are respectively the airgap and iron average lengths of flux path, for each position, and are given by the following equations if $0<x<0.5\tau_S$:

$$l_g(x)=2(g+h_s)-\frac{4h_s\,x}{\tau_s} \qquad (28)$$

$$l_f(x)=2\big(h_p+2(g+h_s+w)\big)-l_g(x) \qquad (29)$$

Fig. 4 illustrates the airgap average length of flux path versus relative position characteristic, considering g=3mm and b_P=18mm. Note that both x=0 and $x=\tau_S$ are unaligned positions, whereas $x=0.5\tau_S$ is the aligned position.

For exemplification purposes, in addition Fig. 5 shows the magnetization characteristics of the future selected prototype. As can be seen, the lookup table values of the magnetization characteristics are stored in the form of necessary current in a phase to achieve a specific value of linkage flux for a given position.

5 Design results

As an example a prototype was designed with the following requirements:

- rated speed: 10 m/s
- developed force at rated speed: 60N
- supply voltage: 200V

For this design analysis the airgap was set in steps of 1mm and the primary teeth length was set in steps

Airgap average length of flux path versus relative position characteristic

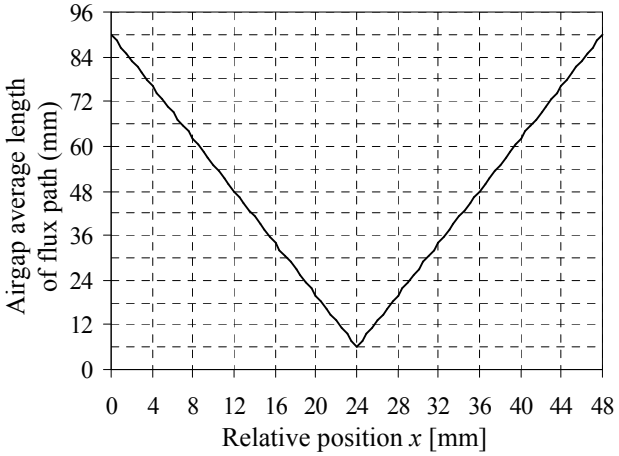

Fig.4 Airgap average length versus relative position.

Graphic representation of the machine magnetization curves lookup table

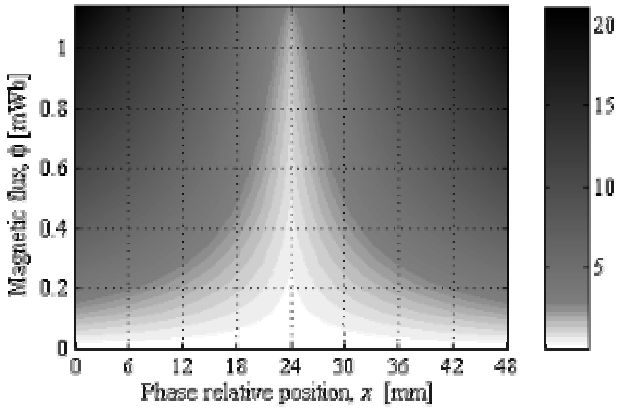

Fig.5 Phase current [A] versus relative position and flux linkage (magnetization curves).

Graphic representation of the stored magnetic energy, W_m, concerning one phase magnetic circuit

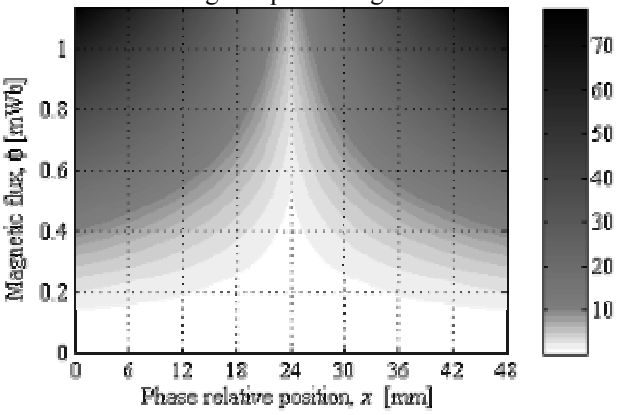

Fig.6 Stored magnetic energy [Joule] versus relative position and flux linkage, for one machine phase.

of 3mm in order to obtain measurable values of the secondary pole pitch.

The winding wire diameter D_{cu} was chosen with the standard value of 0.5mm, and as can be seen

before, each phase winding is composed by 4 parallel connected coils, thus $N_r = 4$.

The number of turns per coil was set in steps of 80 because one wants to use this prototype for fault tests.

It can be seen in Fig. 7 (all machines with no sufficient force or with high current are not display for clearly), that the b_p and g must be as smaller as possible in order to maximize efficiency. In addition, by considering the selected values of 3mm and 18mm for g and b_P respectively, Fig. 8 shows the influence of both N_e and w on the most significant remaining machine dimension, that is the machine height, and on the machine developed force, the last the most important of the remaining performance parameters.

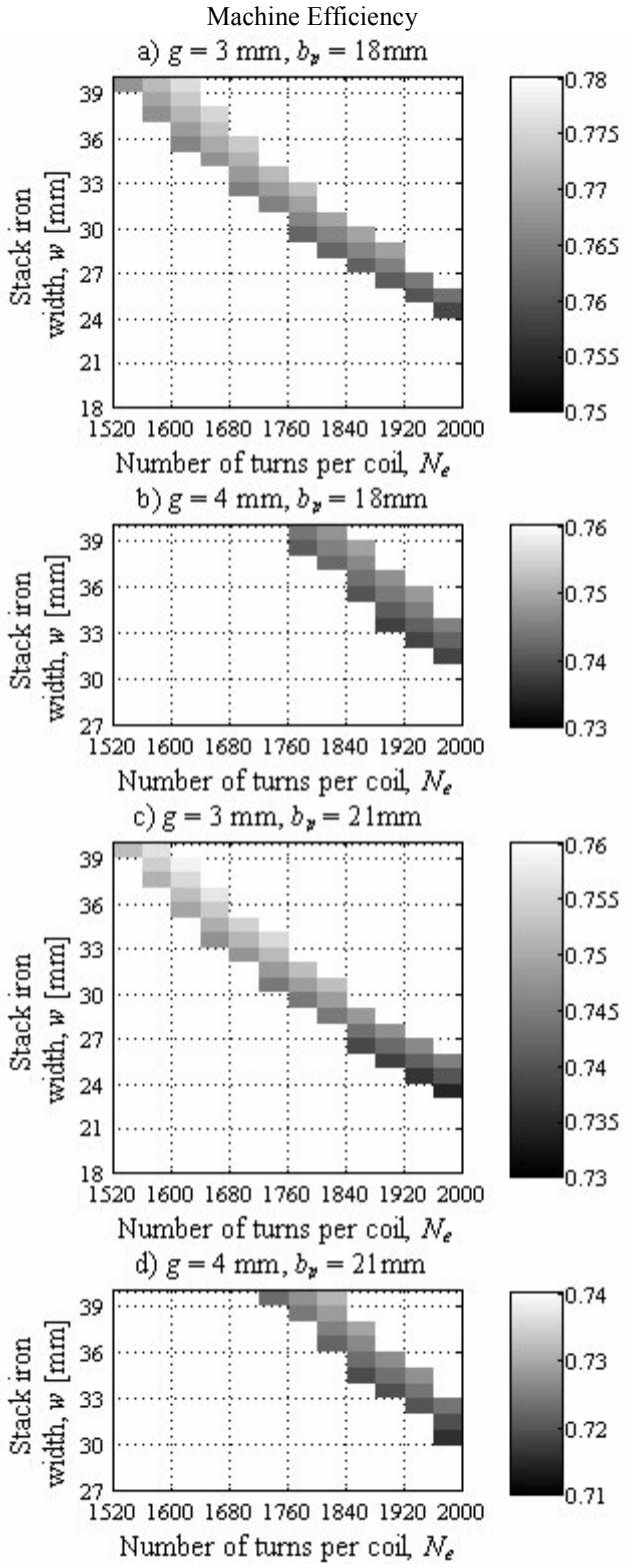

Fig.7 Machine efficiency as a function of N_e and w for several combinations of g and b_P.

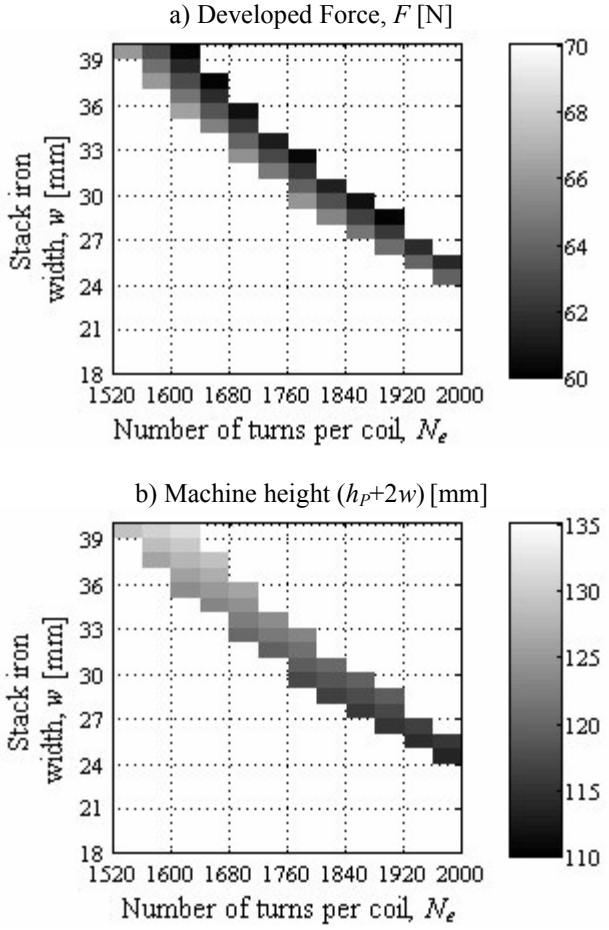

Fig.8 Influence of N_e and w on the machine performance and dimensions.

In authors´ opinion, the most suitable machine for selected traction application should have the following dimensions:

- b_P=18mm
- g =3mm
- w =33mm
- N_e=1680 turns

In order to evaluate if the selected D_{cu} value is the most suitable, Table 1 and Table 2 present several winding configurations. Note that, for the same slot fill factor and current density in the copper, and independently from D_{cu}, the necessary winding develops similar force with similar efficiency.

Table 3 shows the results obtained from the proposed design process, and a general view of the machine can be seen in Fig. 9.

Figs. 10 to 12 show the expected machine performance, respectively for constant speed and constant traction effort (at both start and steady states), and assuming the design setup, i.e.:

- supply voltage equal to 200 V,
- X_0 equal to 0,
- X_C equal to $0.4\tau_S$,
- single pulse control between X_0 an X_C,
- traction effort of 60 N at a speed of $10 ms^{-1}$.

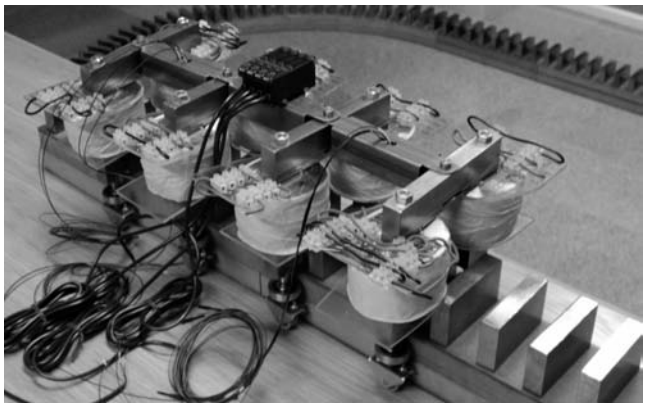

Fig.9 General view of the LSRM prototype.

Table 1 Different winding topologies for the prototype, as a function of some dimensional characteristics.

	Slot fill factor, K_e [%]			Number of turns per primary coil, N_e		
	D_{cu} [mm]			D_{cu} [mm]		
N_r	0.2	0.5	0.8	0.2	0.5	0.8
1	7.95	24.11	40.38	6680	3240	2120
2	12.38	35.12	48.76	5200	2360	1280
4	18.67	50.00		3920	1680	640
6	23.71			3320		
22	48.19			1840		
24	48.00			1680		

Table 2 Different winding topologies for the prototype, and influence on the machine performance.

	I_{pu}			Eficiency, η [%]			Force, F [N]		
	D_{cu} [mm]			D_{cu} [mm]			D_{cu} [mm]		
N_r	0.2	0.5	0.8	0.2	0.5	0.8	0.2	0.5	0.8
1	0.905	0.911	0.916	34.57	62.49	73.05	1.44	13.93	38.37
2	0.906	0.925	1.132	46.13	70.40	76.85	3.65	29.88	86.73
4	0.912	0.962		56.51	76.78		8.43	63.91	
6	0.901			62.12			13.18		
22	0.907			76.17			52.91		
24	0.997			76.10			63.42		

Table 3 Design results for the prototype geometric dimensions.

Required performance		Geometric design input data (Cont.)		Geometric design output data (Cont.)	
F_{ref} [N]	60	N_2	6	l_b [mm]	24
v [m/s]	10	D_{cu} [mm]	0,5	h_b [mm]	50
Geometric design input data		w [mm]	33	b_s[mm]	18
m	4	N_e	1680	I_{max} [A]	0.69
V_0 [V]	200	Geometric design output data		C_m [mm]	461
g [mm]	3	τ_S [mm]	48	l_m [mm]	203
b_p [mm]	18	h_p [mm]	57	Simulation results	
N_r	4	h_s [mm]	42	I_{pu}	0,96
N_{br}	1	τ_p [mm]	132	F_{med} [N]	64
				η	0,77

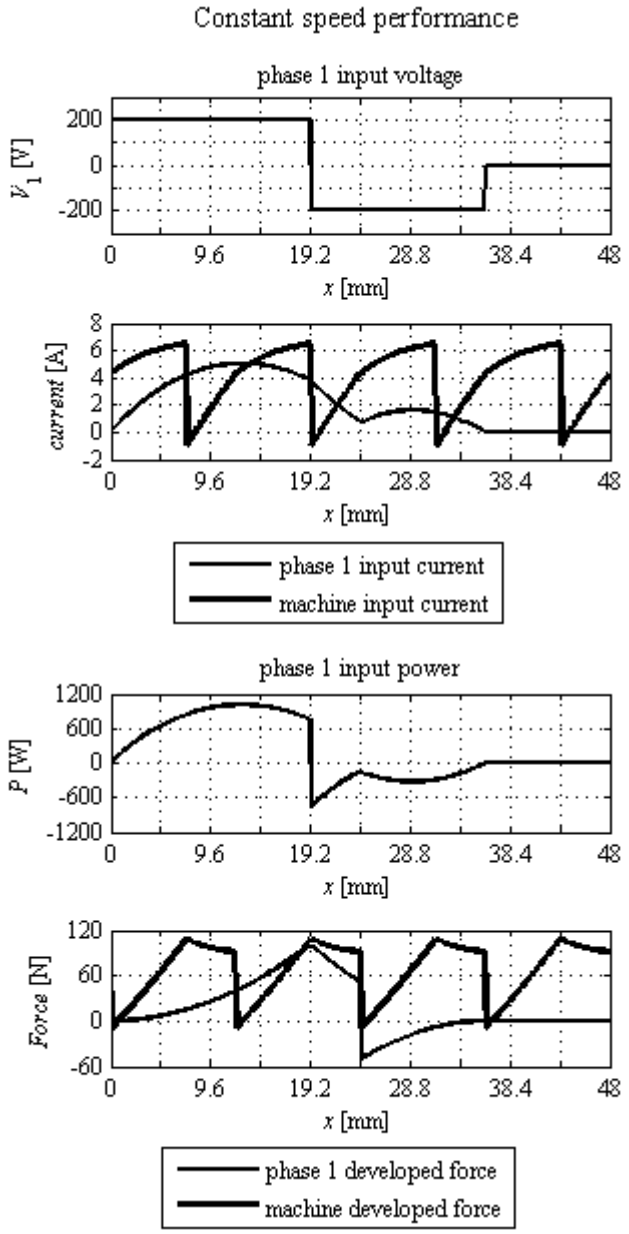

Fig.10 Expected performance at a constant speed of 10 ms^{-1}.

Note that the start position is the unaligned position of phase 1, thus start is provided only by phase 4.

The slight over-dimensioning of the machine can be seen in Fig. 12, since, for one traction effort of 60N the rated speed is slightly over 10ms^{-1}.

6 Conclusions

The proposed methodology, concerning LSRM design, is a good contribution and a strong advantage. This method is faster than others based on finite element method and more accurate than analytical design. It saves engineering costs, producing also good approximations at first attempt, and provides convenient learning and simulation facilities.

It was proved that the value of the winding wire diameter doesn't change the rest of the machine dimensions or the global performance.

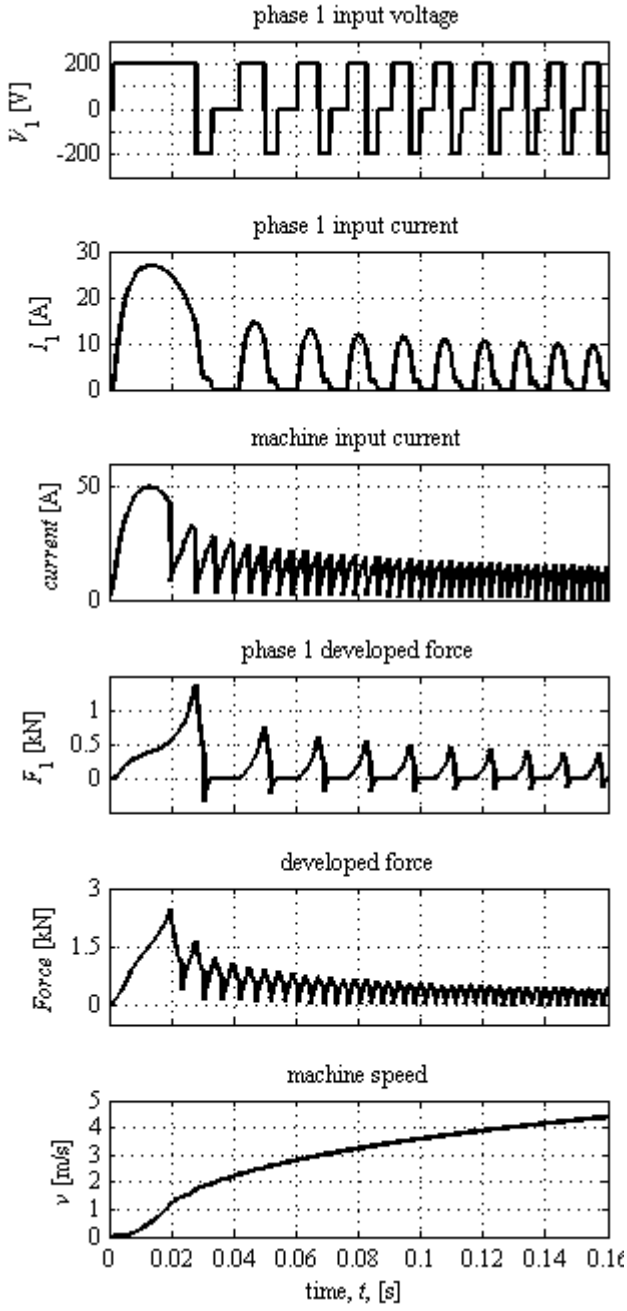

Fig.11 Startup of the machine.

Acknowledgments

The authors would like to thank the financial support provided by the University of Beira Interior and the CASE-Centro de Accionamentos e Sistemas Eléctricos da Fundação para a Ciência e a Tecnologia (FCT) of Portugal.

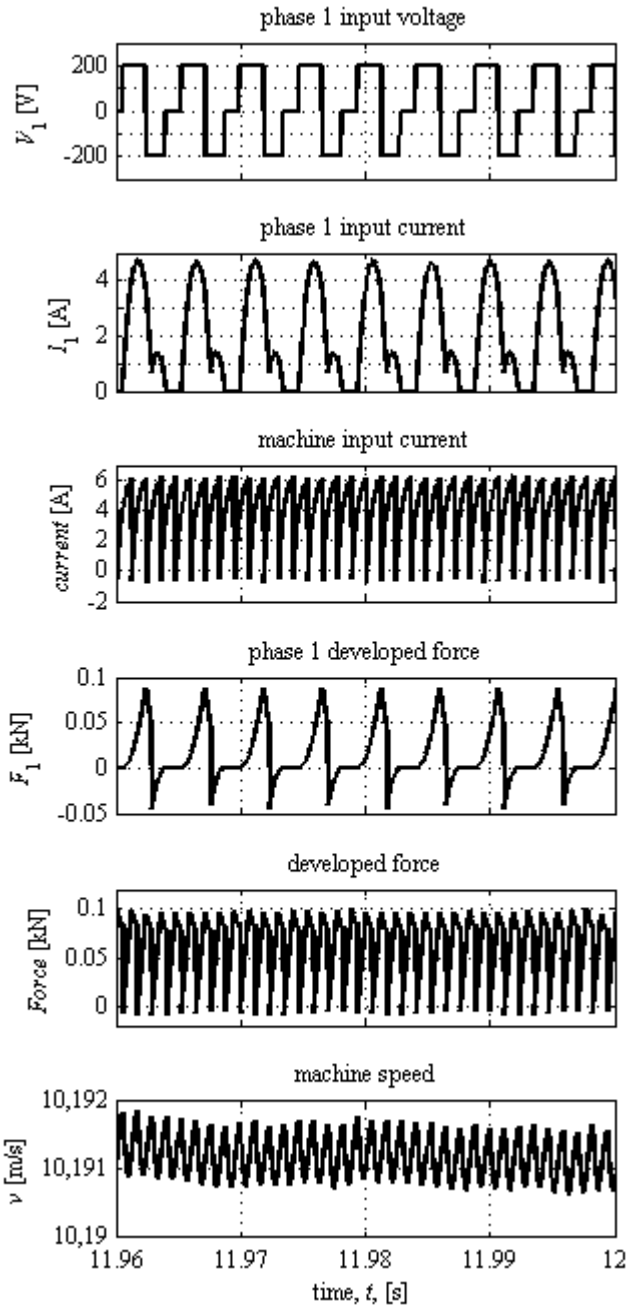

Fig.12 Rated regime performance.

References:

[1] T.J.E. Miller, *Switched Reluctance Motors and their Control*, Oxford, UK: Magna Physics Publishing and Clarendon Press, 1993.

[2] D.S.B. Fonseca, C.P. Cabrita, M.R.A. Calado, Linear Switched Reluctance Motor. A new Topology for Fault Tolerant Traction Applications, *Proceedings of the 2005 IEEE International Electric Machines and Drives Conference IEMDC'2005, San Antonio, Texas, USA*, May 15-18, 2005, pp. 823-827.

[3] Nicholas J. Nagel and Robert D. Lorenz, Modeling of a Saturated Switched-Reluctance Motor Using an Operating Point Analysis and the Unsaturated Torque Equation, *IEEE Trans. on Industry Applications*, Vol. 36, No. 3, May/June 2000, pp. 714-722.

[4] C. Cossar and T.J.E. Miller, Electromagnetic Testing of Switched Reluctance Motors, *Proceedings of the International Conference on Electrical Machines ICEM'92*, Manchester, UK, September 14-17, 1992, pp. 470-474.

[5] D.S.B. Fonseca, C.P. Cabrita, M.R.A. Calado, Linear Switched Reluctance Motor. A New Design Methodology Based on Performance Evaluation, *IEEE International Conference on Industrial Technology ICIT'2004*, *Yasmine, Hammamet, Tunisia*, December 8-10, 2004, paper TF-001696.